Numerical Methods in Civil Engineering, 7-1 (2022) 37-56

Numerical Methods in Civil Engineering

Journal Homepage: https://nmce.kntu.ac.ir/

Investigation of flexural behavior of reinforced concrete beams using 3D finite element analysis

FNU Tabish[*], Ali Raza[**], Shafiullah[***] and Muhammad Sohail Jameel[****]

ARTICLE INFO

RESEARCH PAPER

Article history:
Received:
August 2021.
Revised:
February 2022.
Accepted:
March 2022.

Keywords:
3D Finite Element Analysis,
Reinforced Concrete Beam,
ANSYS,
FE Modelling,
Shear span to Depth Ratio,
Crack Identification

Abstract:

Many experimental works available in the literature explore the structural behavior of flexural members, but a limited number of studies examined the structural behavior of flexural members using nonlinear finite element modeling (FEM). The purpose of the present study is to investigate the effect of reinforcement ratio as well as shear span on the flexural and shear behavior of reinforced concrete beams using three-dimensional FEM in ANSYS. Experimental data and results of fifty-five reinforced concrete beams were compared. Concrete was modeled using a three-dimensional SOLID65 solid element, capable of representing the actual behavior of nonlinear brittle materials such as concrete. Discrete reinforcement was modeled using a three-dimensional LINK180 spar element. The outcomes of the finite element model for loading and cracking of flexural members with a discrete modeling approach were in good agreement with theoretical and experimentally obtained results at all stages of loading. Furthermore, it was observed that at the early stage, the finite element model shows a nearly close result to experimental data compared to the result obtained at the ultimate stage. The outcomes of this study are of utmost importance for structural engineers in designing reinforced flexural members.

1. Introduction

A structure is a combination of different components used to support loads. The prediction of the performance of these structural components under a variety of loadings is essential for a capable and economic structure. Although experimental testing approaches for the response of these structural components can provide significant results, they can be time-consuming, costly, and sometimes impossible, especially for larger and complex civil engineering structures. especially for larger and complex civil engineering structures. An approach to predicting the performance of these structural components is the finite element modeling (FEM) technique. FEM is one of the numerical approaches established on using the nonlinear behavior of materials to accurately predict their complex damaging response [1-9]. The performance of reinforced cement concrete (RCC) and prestressed concrete members can be accurately predicted using FEM [10-13]. Nowadays, the use of FEM software such as ANSYS, Abaqus, Strand7, and Siesmostruct has been increasing because of the advancements in the computational fields [14-19]. The advancement of finite element (FE) computer software does not mean there is no need for experimental data at all, but to thoroughly understand the efficiency of FE computer software, we must study the experimental data. Also, the experimental-based tests provide a base to understand the working of FEM code clearly. Over the last few decades, more comprehensive

* *University of North Dakota (UND), Grand Forks, ND 58203 USA; E-mail: tabish.naseer@und.edu*

** *Corresponding author: Department of Civil Engineering, University of Engineering and Technology Taxila, 47050, Pakistan; E-mail: ali.raza@uettaxila.edu.pk*

*** *Case Western Reserve University, Cleveland, Ohio, 44106, USA; E-mail: sxu79@case.edu*

**** *Department of Transportation Engineering and Management, University of Engineering and Technology Lahore, 54890, Pakistan; E-mail: sohail.jameel@uet.edu.pk*

https://doi.org/10.61186/NMCE.2022.343

studies have been carried out on both numerical and experimental examinations of the response of RC beams. A few of them are summarized below:

Wolanski [20] investigated the flexure response of beams made of reinforced and prestressed concrete using ANSYS. An RC beam was analyzed under a four-point bending test. The cracking pattern in the RC beam was identified at different stages. The results obtained from nonlinear 3D FEM of the RC beam were compared with experimental results on a control beam presented by Buckhouse [21]. The FEM results were in close agreement with the experimental results as well as with the theoretically calculated results.

Dahmani et al. [22] studied the scope of the ANSYS software for investigating fracture patterns in the light RC beams. Cracks were identified at stages of initial cracking, beyond initial cracking, yielding of steel, beyond steel yielding, and strength limit state under one-point loading. In the end, a comparison was made between the results of FEM of RC beams and results obtained from the theoretical evaluation. A good agreement between the testing results and FEM predictions was obtained.

Khan et al. [23] examined the shear behavior of RC beams using ANSYS software. The results acquired from the 3D FEM model were evaluated with results from experimental testing on an RC beam carried by Tahenni et al. [24]. The FEM results matched the experimental results with high accuracy. Some researchers, such as Carpinteri et al. [25] and Badiger et al. [26], evaluated the effect of different percentages of steel reinforcement on the crack propagation, the shape of the fissures, and the relation to the mode of failure of the beam using ANSYS.

Numerous researches have been conducted to evaluate the impact of variation in shear span to depth ratio (a/d ratio) on shear and flexural behavior of RC and ultra-high-performance concrete beams using the FEM approach [27-31]. The results obtained from FEM models were also validated with experimental work with satisfactory results. Though much research on FE modeling has already been published, there is still a need to investigate the RC beams for their cracking and failure mechanism under flexural loads while considering the maximum parameters of FEM and RC beams in a single research.

In this study, a total of fifty-five RC beams were modeled to investigate the impact of reinforcement and shear span to depth ratio on the flexural strength, shear strength, and cracking patterns of RC beams using the ANSYS software. Also, the results obtained from the ANSYS software were compared with experimentally tested RC beams which were not addressed yet in the literature, becoming the novelty of the present work, including the parametric study.

The primary objectives of the present study are the following:

1. To propose an accurate FEM model for predicting the structural behavior of RC beams using state-of-the-art FEM techniques.
2. To evaluate the effects of shear span and steel ratio on the shear and flexural strength of RC beams.
3. To investigate the impact of reinforcement and shear span to depth ratio on the flexural strength, shear strength, and cracking patterns of RC beams.
4. To examine and compare the cracking behavior and failure model of RC beams.
5. To compare the results obtained from the proposed FEM model with experimental results of RC beams;
6. To compare the relative flexural capacity of each FEM model with the relative flexural capacity obtained from the experimental testing of RC beams.

2. Experimental Work

The reference selected to make RC beams for this investigation was the research carried out by Elahi [32]. This investigation tested a total of fifty-five R.C beams without web reinforcement. All beams had the same cross-section of 6″×12″. The RC beams, made of high-performance concrete, were studied in five groups with varying steel ratios. Each group contained eleven beams with shear span to effective depth ratio (a/d) varied from 1-6 with an increment of 0.5, as shown in Table 1.

All beams were subjected to single point loads at their middle points. The geometric specifications of the test specimen are shown in Figure 1.

3. Finite Element Modeling

The reinforced concrete beams are taken and analyzed by FEM using the commercially available software ANSYS 14.5.

3.1 Element Types

Concrete is modeled by a 3-D solid element named SOLID65. It is described with eight nodes, each possessing three degrees of freedom (DOF) of translations in x, y, and z nodal directions. This solid element can describe crushing, cracking in each orthogonal direction, and plastic deformation. The fracture process of concrete was defined using the constitutive model proposed by William and Warnke [33].

A 3D spar element LINK180, consisting of two nodes with three DOFs at each node (translations in x, y, and z-direction nodal), is used to model the steel reinforcement. It can undergo plastic deformation. The steel reinforcement for the FEM has been assumed to be an elastic-perfectly plastic material and equal under tensile and compressive loads.

Table 1: General Group Data

Group #01 ρ = 0.349 %		Group #02 ρ = 0.635 %		Group #03 ρ = 0.984 %		Group #04 ρ = 1.397 %		Group #05 ρ = 1.937 %	
Beam Type	**a/d**	**Beam Type**	**a/d**	**Beam Type**	**a/d**	**Beam Type**	**a/d**	**Beam Type**	**a/d**
BF1	1	BG1	1	BH1	1	BI1	1	BJ1	1
BF2	1.5	BG2	1.5	BH2	1.5	BI2	1.5	BJ2	1.5
BF3	2	BG3	2	BH3	2	BI3	2	BJ3	2
BF4	2.5	BG4	2.5	BH4	2.5	BI4	2.5	BJ4	2.5
BF5	3	BG5	3	BH5	3	BI5	3	BJ5	3
BF6	3.5	BG6	3.5	BH6	3.5	BI6	3.5	BJ6	3.5
BF7	4	BG7	4	BH7	4	BI7	4	BJ7	4
BF8	4.5	BG8	4.5	BH8	4.5	BI8	4.5	BJ8	4.5
BF9	5	BG9	5	BH9	5	BI9	5	BJ9	5
BF10	5.5	BG10	5.5	BH10	5.5	BI10	5.5	BJ10	5.5
BF11	6	BG11	6	BH11	6	BI11	6	BJ11	6

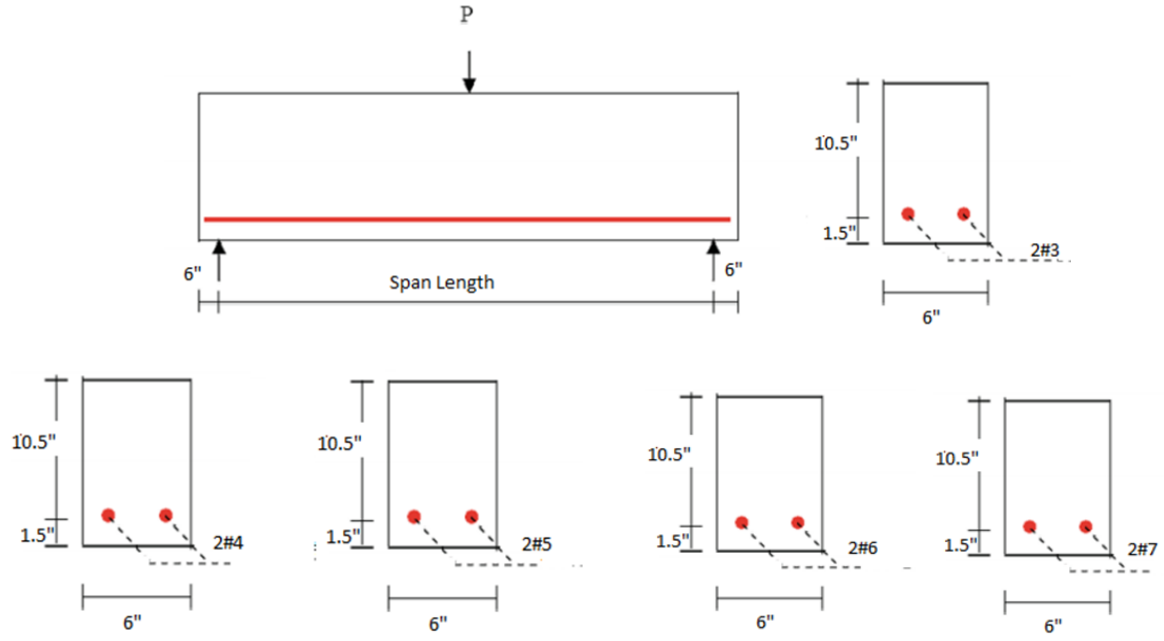

Fig. 1: Geometrical details of the test specimen

3.2 Real Constants

Some properties, such as the cross-sectional properties of RC beam elements, are real constants that depend on the type of material, noting that real constants are different for individual elements. For these working models, real constants are presented in Tables 2-3.

Real Constant Set 1 is defined for the SOLID65 element. The stiffness and orientation of reinforcement are defined by the user. In the present study, discrete reinforcement is used to model the connection. As suggested by previous studies, a zero value was entered to turn off the smeared capacity of steel reinforcement for the SOLID65 element [34-36].

For the analysis of the LINK180 element, a real Constant Set 2 is assigned. Values for the cross-sectional area and initial strains were entered. There are five groups concerning reinforcement ratio; therefore, the cross-sectional area in Set 2 refers to the steel bars of #3, #4, #5, #6, and #7 diameter, respectively. A zero value was entered in the table for the initial strain because there was no initial stress present in the reinforcement.

Table 2: Real Constant Set 01 for the Working Models

Group No.	Set of Real Constant	Type of Element	Constant			
			Parameter	Real constant for rebar 01	Real constant for rebar 02	Real constant for rebar 03
All Groups	1	SOLID65	Material No.	0.0	0.0	0.0
			Ratio of Volume	0.0	0.0	0.0
			Orientation Angle	0.0	0.0	0.0
			Orientation Angle	0.0	0.0	0.0

Table 3: Real Constant Set 02 for Calibration Model

Group No.	Set of Real Constant	Type of Element	Area and strain	Constants
1	2	LINK180	Area of Cross section (in^2)	0.11
			Initial Strain (in./in.)	0
2	2	LINK180	Area of Cross section (in^2)	0.2
			Initial Strain (in./in.)	0
3	2	LINK180	Area of Cross section (in^2)	0.31
			Initial Strain (in./in.)	0
4	2	LINK180	Area of Cross section (in^2)	0.44
			Initial Strain (in./in.)	0
5	2	LINK180	Area of Cross section (in^2)	0.61
			Initial Strain (inch/inch)	0.0

3.3 Material Properties

Parameters needed for defining the models of material to be used in control specimens are given below in Table 4. SOLID65 element is represented by Material Model Number 1. For the proper modeling of the concrete, linear and multilinear isotropic properties of the material are required by the SOLID65 element. ANSYS needs some material properties data, which is given in Table 4.

For material properties of concrete: Modulus of elasticity (E_c); Ultimate uniaxial compressive strength (f'_c); Modulus of rupture or ultimate uniaxial compressive strength (f_r); Poisson's ratio (v); Coefficient of shear transfer (βt); Uniaxial Compressive stress-strain relationship for the concrete; Elastic modulus (E_c) for concrete is EX, and that PRXY is the Poisson's ratio (v).

A bilinear isotropic LINK180 element is referred to by material model No 2. In the FE model of the beam, LINK180 elements are used for the entire steel reinforcement. According to the research carried out by Shaifullah et al. [37], the von Mises failure criteria is the base of bilinear isotropic material. The bilinear model needs the tensile yield strength (f_y) and modulus of hardening for steel to be assigned. In our models, the elastic limit or yield strength was defined as 60000 lb/in^2, and the modulus of hardening was 2900 lb/in^2. When the crushing ability was turned on, convergence problems were repeatedly observed.

3.4 Interaction and Modeling

The specifications of the full-sized beams were 6.00×12.00 in. The span between the two supports varied from 1 ft 9 in to 10 ft 6 in with an increment of 10.5 in each.

The full scale of RC beams was modeled in the form of small finite elements. First of all, an appropriate number of nodes were generated, meeting the present condition. Then, these nodes were joined to form finite elements according to the requirements, as shown in Figure 2. The interaction between the reinforcement and concrete was defined by assuming a perfect bonding between their elements. LINK180 elements of reinforcement were perfectly connected to SOLID65 elements to transfer all required degrees of freedom.

Table 4: Properties of concrete and steel required for FE model

Type of Element	Material Properties	
Linear Isotropic properties		
EX (E_C)	5135380.512 psi	
PRXY (v_C)	0.2	
Multilinear Isotropic properties		
	Strain	Stress
Point No.1	0.000474	2435.1
Point No.2	0.0007	3426.742
Point No. 3	0.00095	4474.513
Point No. 4	0.0025	7898.527
Point No. 5	0.003161	8117
Concrete		
ShrCf-Open	0.3	
ShrCf-Clos	1	
UnTenslSt	668.64 psi	
UnCrushSt	-1	
BiCrushSt	0	
HydroPres	0	
BiCrushSt	0	
UncrushSt	0	
Linear and Bilinear Isotropic properties		
EX (E_S)	29000000 lb/in^2	
PRXY(v_S)	0.30	
Yield Stress f_y	60000 lb/in^2	
Tang. Mod	2900 lb/in^2	

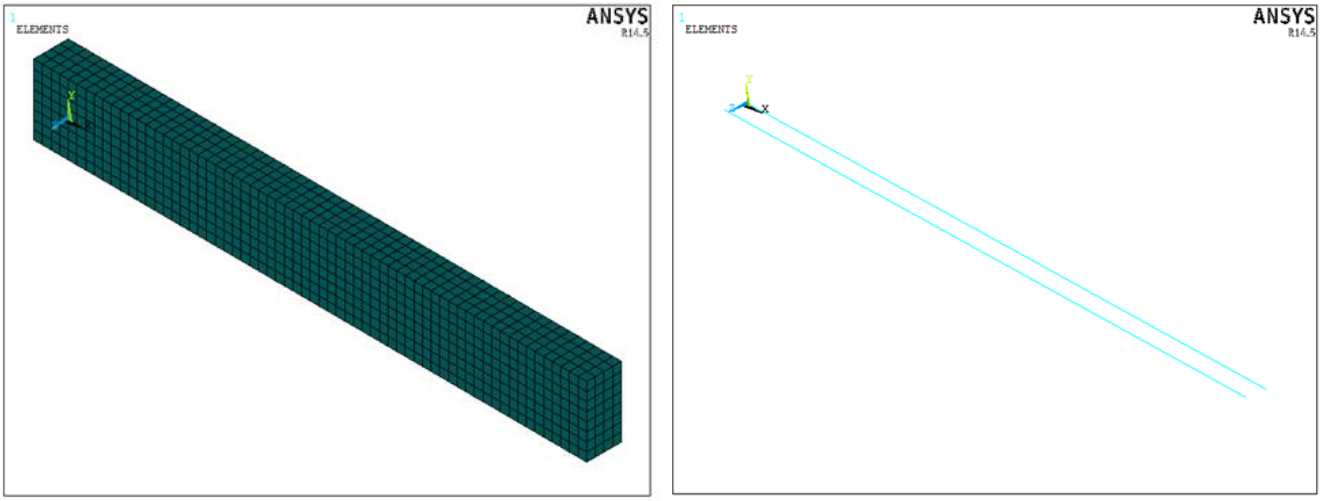

(a) (b)

Fig.2: (a) RC Beam created for FE model (b) Reinforcement developed in FE model

Nodes at a distance of 6 inches from the left end of the RC beams were restrained in X and Y directions, and those from the right end were restrained in the vertical direction. LINK180 elements were used to form the flexural or bending reinforcement. No shear stirrups were considered in the beam because, in the experimental testing of specimens, no stirrups were provided in the beams for the shear reinforcement. Two bars are present in each beam model. Reinforcement details in the discrete model developed by ANSYS are shown in Figure 2.

3.5 Meshing

Meshing is essential to achieve good FEM results. The rectangular mesh is suggested to obtain a better response from the SOLID65 element. No separate mesh for reinforced bars was needed because nodes of reinforced elements were connected to those of adjacent concrete solid elements to satisfy the perfect bond assumption. The size of meshing along the length and depth of models was taken as 1.5 in, as shown in Figure 3. This mesh size was obtained using a mesh sensitivity analysis portraying the highest accuracy at this element size, and hence, it was selected for further analysis of the RC beams.

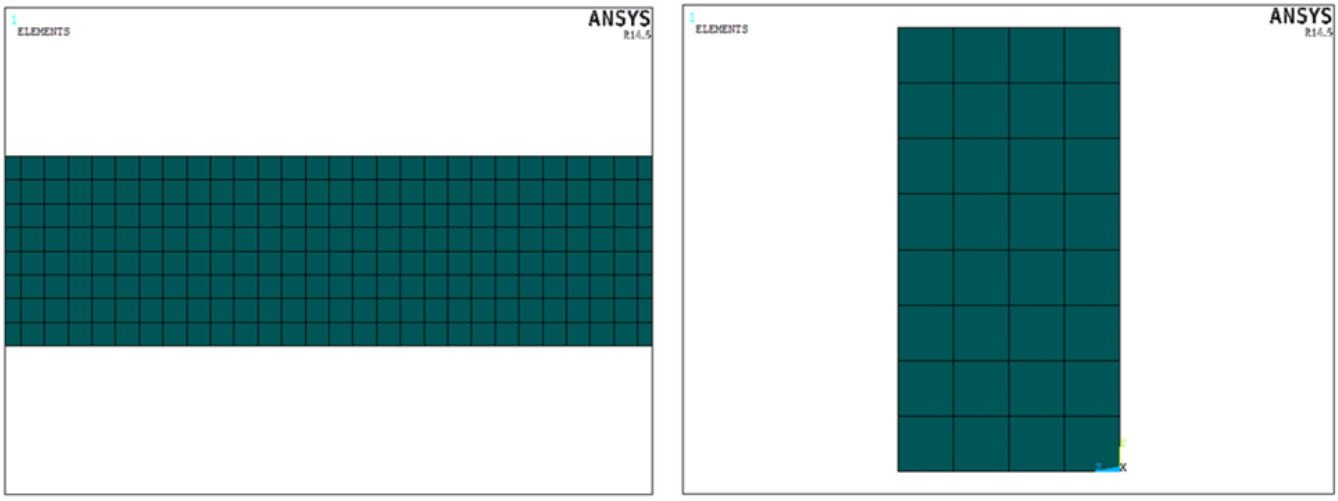

Fig. 3: Meshing size along the length and depth of the FE model

3.6 Boundary Conditions and Loads

In the present study, hinge support was created at the left end of models at a distance of 6 in. Nodes at a 6 in distance from the left end of models were allotted constraint in UX and UY directions with a zero-constant value for producing the hinge support. Roller support was created at the same distance from the right end of the models by assigning constraints in the UY direction with a zero-constant value to the nodes located at that position. A concentrated load was applied at the center of each model. The load applied at each node at the loading position was one-fifth of the actual load. Supporting details and loading conditions are shown in Figure 4.

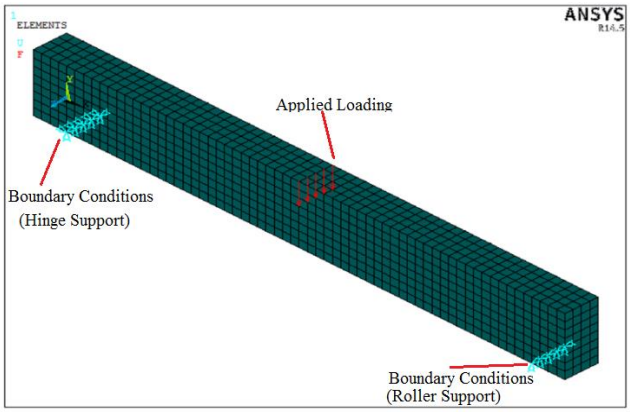

Fig. 4: Support and Loading conditions of FE model

3.7 Analysis Type

To identify fissures in a full-sized RC beam sample, we performed a 3D nonlinear structural analysis on a full-sized beam specimen. ANSYS software solves nonlinear problems by using Newton–Raphson method. In nonlinear analysis, the ultimate load subjected to a FE model is sub-divided into different load increments known as load steps. These load steps are further subdivided into sub-steps. The matrix of stiffness of the specimen was calibrated at the end of the solution of each load step to show nonlinear changes in stiffness of the structure before heading to the next load increment. The load increments for a single model are shown in Table 5.

In this research, the criteria for convergence were based on displacement and force. As Vasudevan and Kothandaraman [38] stated, low convergence limits used for analysis require additional trials, subsequently increasing computational time and disk space. The convergence limits do not change model behavior up to the yielding of the steel stage. In the current research, default convergence criteria were used up to the development of the first crack, and after the first crack, the tolerance limit of 0.25 was used for displacement convergence criteria, and force convergence criteria were dropped. Model failure was observed where the solutions failed to converge even with a tiny load increment.

Table 5: Load increments for nonlinear analysis for BF-5

Starting of time	Time at the end of every Load step	No. of Load steps	No. of Sub steps	Increment of Load (lbs)
0	7250	1	1	7250
7250	7500	2	250	250
7500	9500	3	250	2000
9500	11500	4	250	2000
11500	13500	5	250	2000
13500	15500	6	250	2000
15500	17500	7	500	2000
17500	19500	8	500	2000
19500	21500	9	500	2000
21500	22000	10	250	500

4. Results and Discussion

4.1 Behavior at First Cracking

Initial cracking starts nearly at the mid-span of each model. These first cracks, which occurred in the mid-span of models, are flexural. The maximum value of deflection and stress occurred in the mid-span of models during the application of load as expected. Theoretical calculations are carried out to compute the load at which first cracking takes place and corresponding stresses and deflection. These theoretical calculations are shown in Appendix A. The crack/crushing plot option in ANSYS was used to obtain a cracking pattern in beams. To visualize the cracks in the model, the vector mode option is turned on. The first cracking of a single model for each group is shown in Figure 5. Table 6 shows the experimental results of the examined 55 beams.

Comparison of results at initial cracking obtained from the finite element model is made with experimental as well as theoretical calculation results as shown in Figures 6-10.

4.2 Behavior after First Cracking

Crack patterns produced while carrying out the experimental testing were strongly detected and marked on the RC beams, compared with cracking areas produced by FEM models, and are shown in Figures 11-14, which gives a clear picture of the four-point bending behavior of RC beams. Significantly, the crack patterns created by ANSYS are not the actual cracks but conceivable cracking areas.

If we studied in the nonlinear region of response, succeeding cracking occurred as the applied load was increased. Cracking also increased in the constant moment region. With a gradual increase of loads cracking started growing towards the supports. Also, when the load increased beyond the initial cracking load, diagonal tension cracks started to form in the beam model. The cracking behavior after the initial cracking load can be seen in Figures 11-14. When the flexural loading was increased, the cracks in the damaged RC beams increased moving towards the end supports, revealing the cracks were shifting from flexural to shear cracks.

Fig. 5: First cracking of single FE model for each Beam Series

Table 6: The experimental results of the examined beams

Sr. No.	Beam ID	A_s (in)	P_{cr} (Kips)	Deflection (in)	P_u (Kips)	M_f (Kip-in)	Vu (Kips)
1	BF1	0.22	28.11	0.001	43.29	227.28	0.404
2	BF2	0.22	17.31	0.052	25.97	204.48	0.242
3	BF3	0.22	10.82	0.047	15.20	159.60	0.142
4	BF4	0.22	3.90	0.024	8.66	113.64	0.081
5	BF5	0.22	7.36	0.053	9.96	156.84	0.093
6	BF6	0.22	6.49	0.101	9.09	167.04	0.085
7	BF7	0.22	3.90	0.109	6.92	145.32	0.065
8	BF8	0.22	2.16	0.113	6.06	143.16	0.057
9	BF9	0.22	3.90	0.231	5.19	136.20	0.048
10	BF10	0.22	2.60	0.232	4.76	137.40	0.044
11	BF11	0.22	2.16	0.265	3.03	95.40	0.028
12	BG1	0.40	25.96	0.003	43.25	227.04	0.404
13	BG2	0.40	15.14	0.055	36.33	286.08	0.339
14	BG3	0.40	8.66	0.063	34.17	358.80	0.319
15	BG4	0.40	10.82	0.078	25.96	340.68	0.242
16	BG5	0.40	8.66	0.084	21.20	333.96	0.198
17	BG6	0.40	6.49	0.098	15.18	278.88	0.142
18	BG7	0.40	5.63	0.114	13.85	290.88	0.129
19	BG8	0.40	4.33	0.133	16.01	378.24	0.149
20	BG9	0.40	4.33	0.246	11.25	295.32	0.105
21	BG10	0.40	3.03	0.258	10.22	295.08	0.093
22	BG11	0.40	3.46	0.317	8.66	272.76	0.081
23	BH1	0.62	38.98	0.002	86.45	453.84	0.807
24	BH2	0.62	12.98	0.041	38.49	303.12	0.359
25	BH3	0.62	12.98	0.071	41.95	440.52	0.392
26	BH4	0.62	7.79	0.066	22.50	295.32	0.210
27	BH5	0.62	8.66	0.063	17.31	272.64	0.162
28	BH6	0.62	8.66	0.119	19.74	362.76	0.184
29	BH7	0.62	8.66	0.116	21.20	445.20	0.198
30	BH8	0.62	6.49	0.202	18.17	429.24	0.170
31	BH9	0.62	5.63	0.258	16.01	420.24	0.149
32	BH10	0.62	4.33	0.278	16.01	462.24	0.149
33	BH11	0.62	4.33	0.367	13.41	422.4	0.150
34	BI1	0.88	32.46	0.006	84.40	443.10	0.788
35	BI2	0.88	21.64	0.082	78.77	620.28	0.785
36	BI3	0.88	12.98	0.100	63.72	669.04	0.586
37	BI4	0.88	12.98	0.073	51.07	670.32	0.477
38	BI5	0.88	10.39	0.095	24.24	381.84	0.226
39	BI6	0.88	8.22	0.131	20.77	381.6	0.194
40	BI7	0.88	7.79	0.131	20.77	436.20	0.194
41	BI8	0.88	4.33	0.271	20.77	490.68	0.194
42	BI9	0.88	5.63	0.301	21.64	567.96	0.202
43	BI10	0.88	5.63	0.314	23.37	674.76	0.218
44	BI11	0.88	5.63	0.302	22.07	695.16	0.206
45	BJ1	1.22	34.62	0.008	87.86	461.24	0.820
46	BJ2	1.22	23.8	0.083	86.57	681.72	0.808
47	BJ3	1.22	10.82	0.075	60.59	636.24	0.566
48	BJ4	1.22	12.98	0.089	45.01	590.76	0.420
49	BJ5	1.22	11.25	0.097	25.97	409.08	0.242
50	BJ6	1.22	12.98	0.143	23.37	429.48	0.218
51	BJ7	1.22	8.66	0.171	27.27	572.64	0.255
52	BJ8	1.22	8.66	0.280	27.70	654.36	0.259
53	BJ9	1.22	8.66	0.333	25.10	658.92	0.234
54	BJ10	1.22	6.49	0.337	22.51	649.98	0.210
55	BJ11	1.22	6.49	0.415	23.37	736.20	0.218

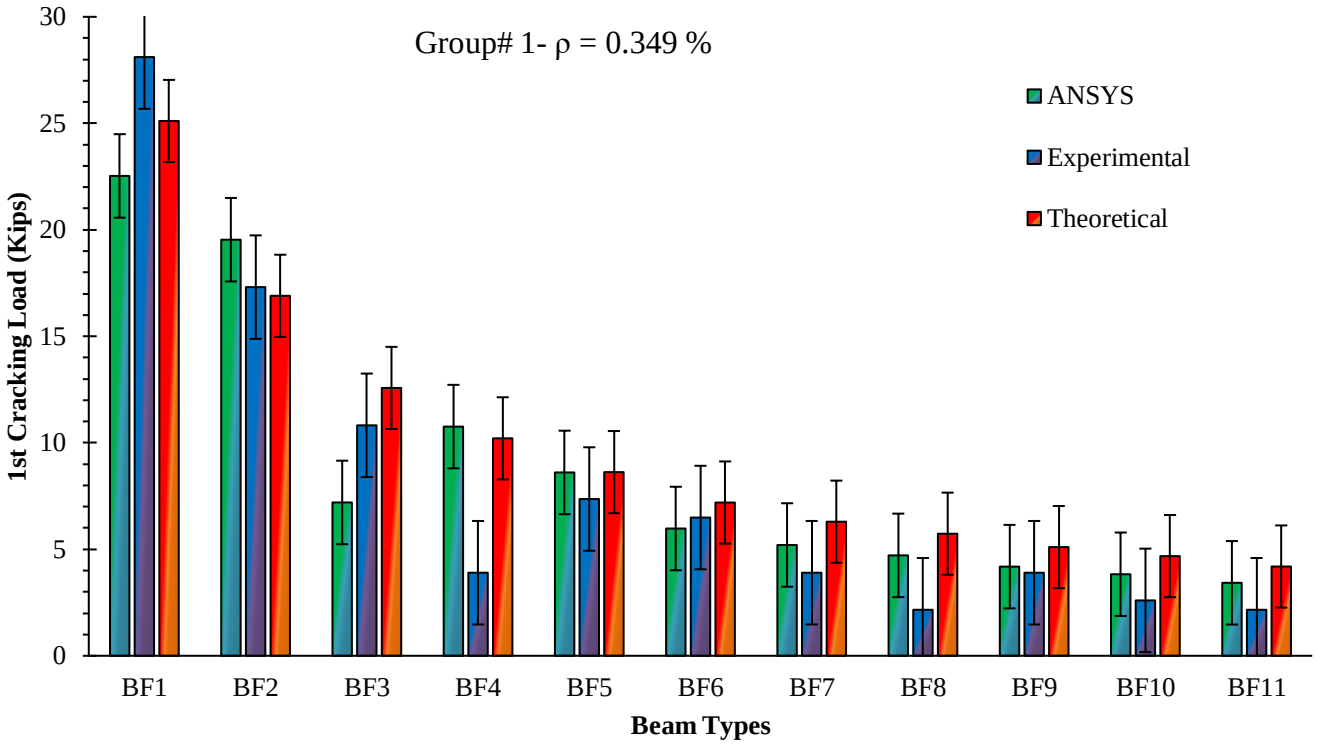

Fig. 6: Comparison of 1st Cracking Load between FEM, experimental and theoretical results for Group No. 01

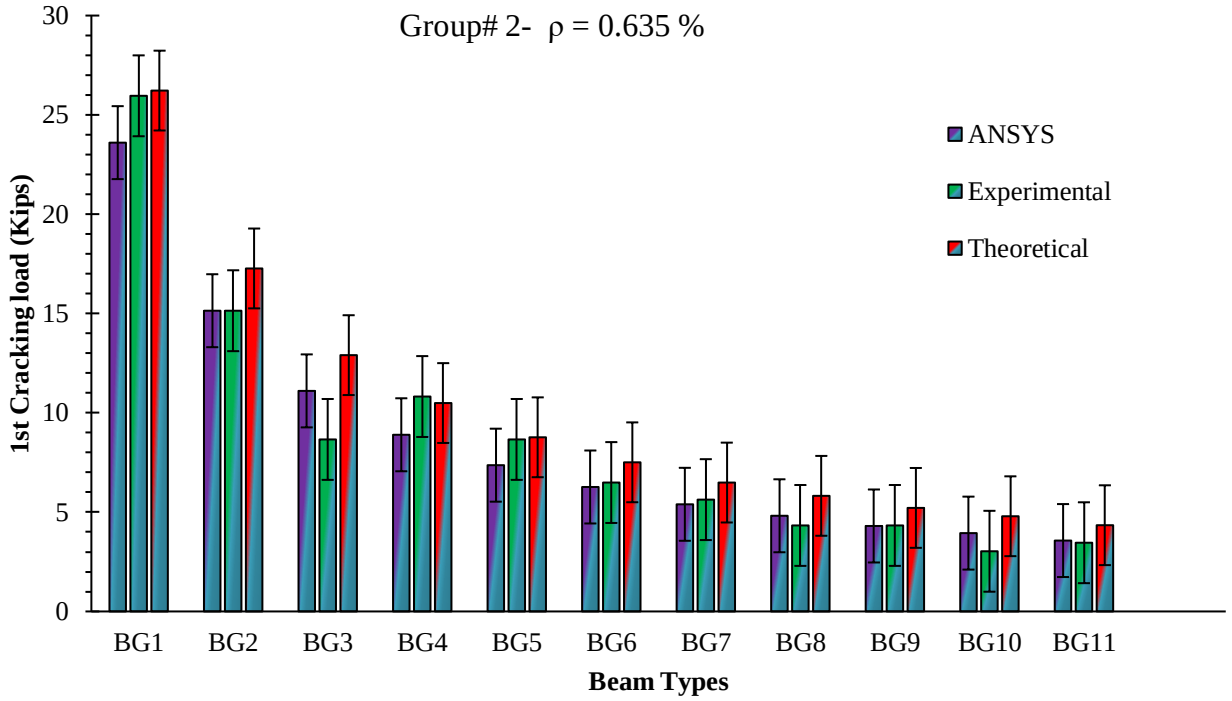

Fig.7: Comparison of 1st Cracking Load between FEM, experimental and theoretical results for Group No. 02

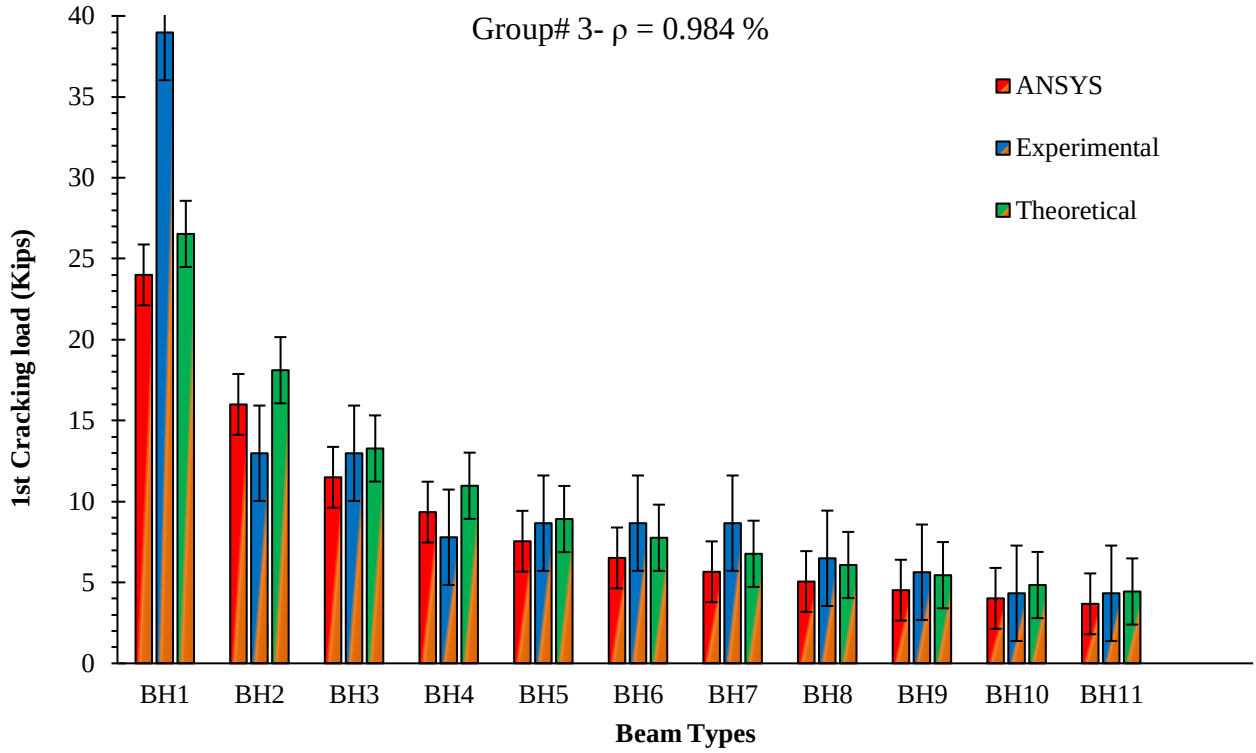

Fig. 8: Comparison of 1st Cracking Load between FEM, experimental and theoretical results for Group No. 03

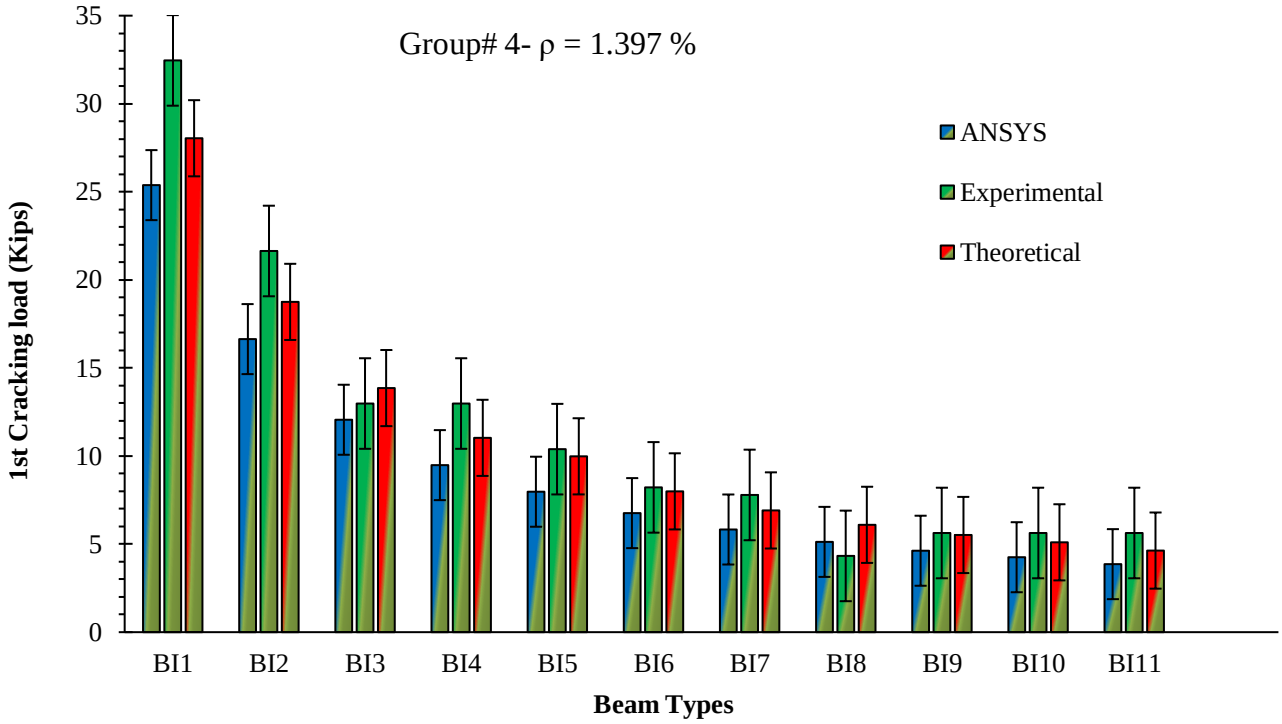

Fig. 9: Comparison of 1st Cracking Load between FEM, experimental and theoretical results for Group No. 04

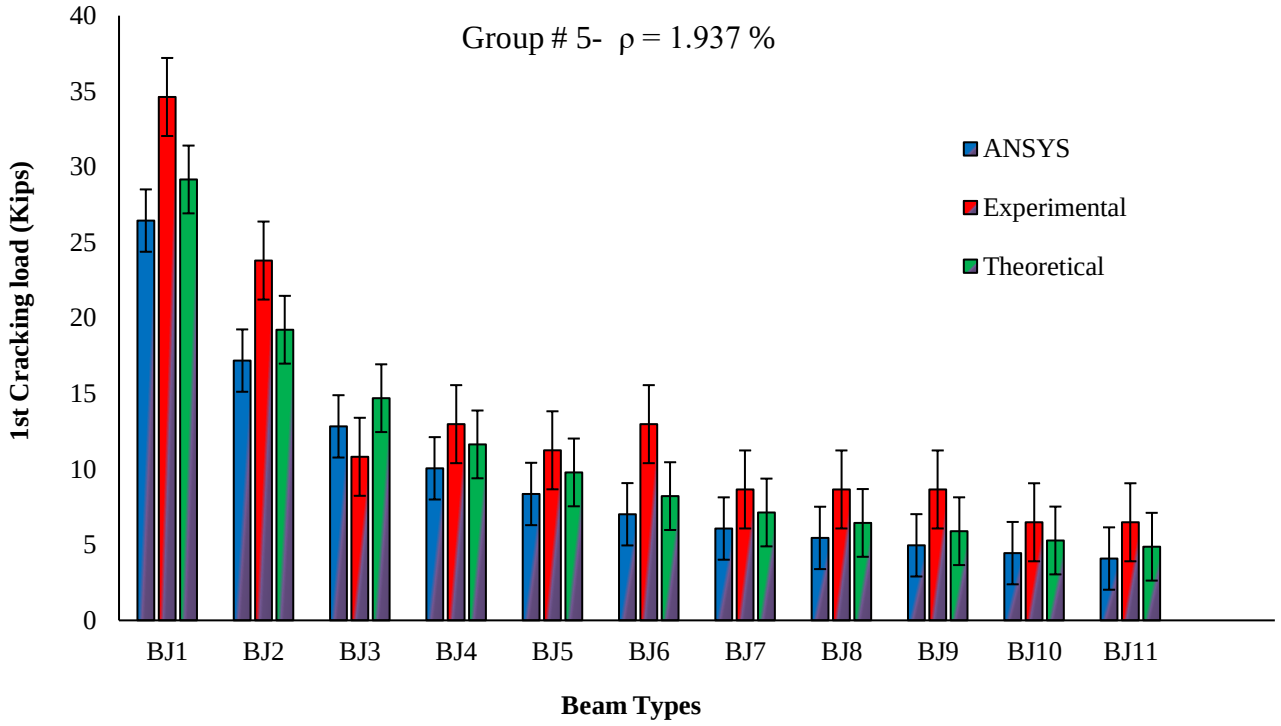

Fig. 10: Comparison of 1st Cracking Load between FEM, experimental and theoretical results for Group No. 05

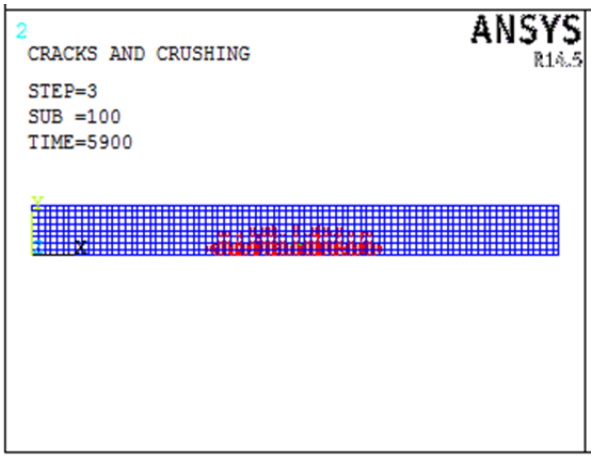

Fig. 11: Cracking of FE model at 5900 lb Load

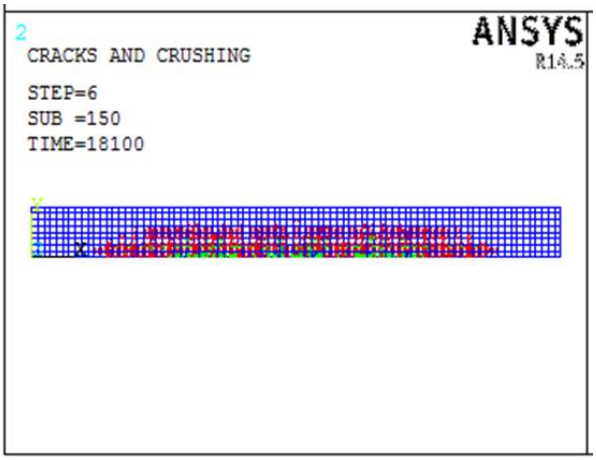

Fig. 13: Increased cracking of FE model beyond yielding of steel

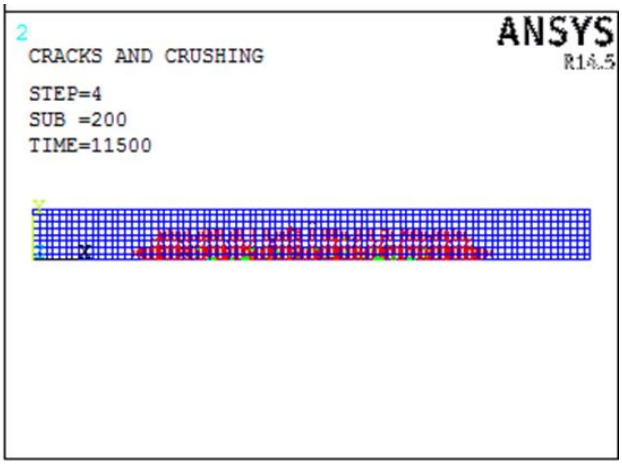

Fig. 12: Further cracking of FE at 11500 lb Load

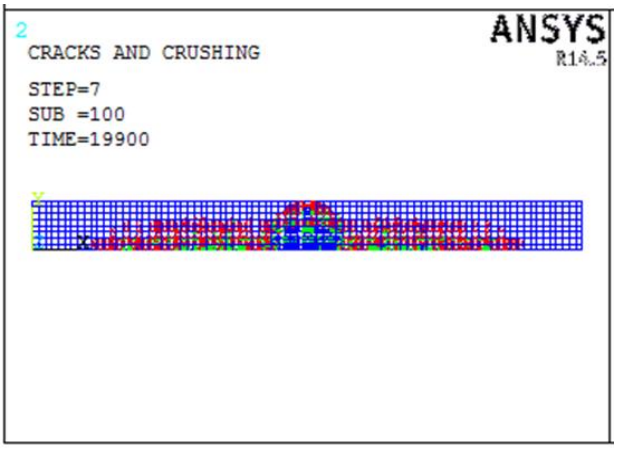

Fig. 14: Cracking just before failure

4.3 Behavior at Strength Limit State

At failure load, the beam cannot support further load, as pointed out by a non-convergence failure. Several cracking all over the entire beam occurs. It is observed that the spreading of cracking increases with the increase of the reinforcement ratio. As in the present study, the reinforcement ratio increases from Group 01 to Group 05, and therefore spreading of cracks increases accordingly, as shown in Figure 15, which shows the failure of the same span beam with varying reinforcement. Severe cracking through the whole constant moment area happens. Remarkable is that just before the failure, a few splitting (compressive) cracks seem at the upper part of the RC beam because of the crushing failure of the concrete.

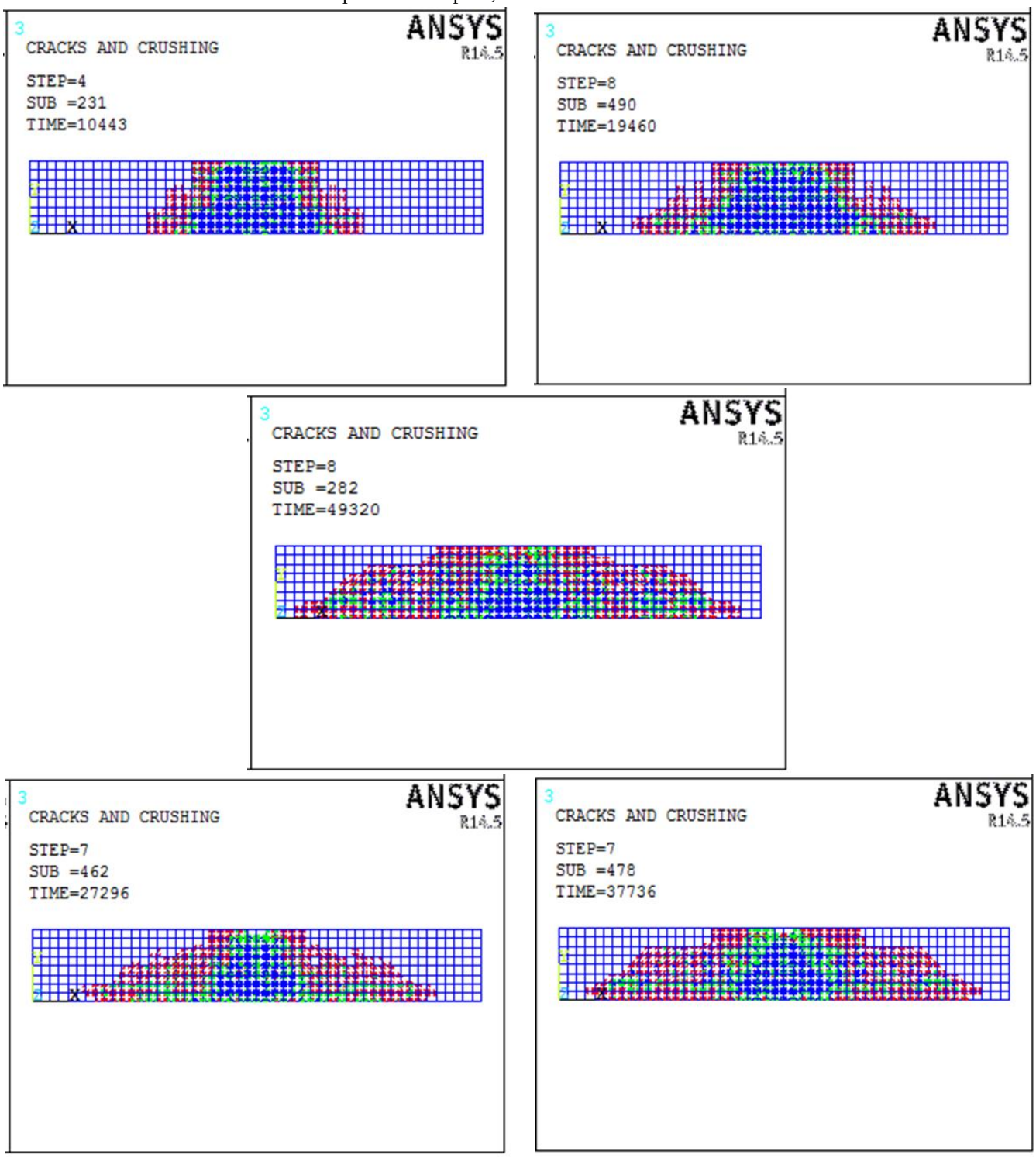

Fig. 15: Cracking of FE model at failure for each Group (from Group 01 -05)

Comparison of results at Strength Limit State obtained from FEM model is made with experimental as well as theoretical calculation results as shown in Figures 16-20. The theoretical calculations for the ultimate capacity of RC beams are presented in Appendix A. Yielding of steel reinforcement occurs when a force greater than its yield strength is applied. At this point, the displacements of the beam start to ameliorate at a more significant rate as more loads are applied. The yielding steel, a cracked moment of inertia, and nonlinear concrete now express the flexural rigidity of the RC beams. The capability of the RC beam to dispense load through the cross-section has lessened momentously. Consequently, larger deflections occur at the beam centerline.

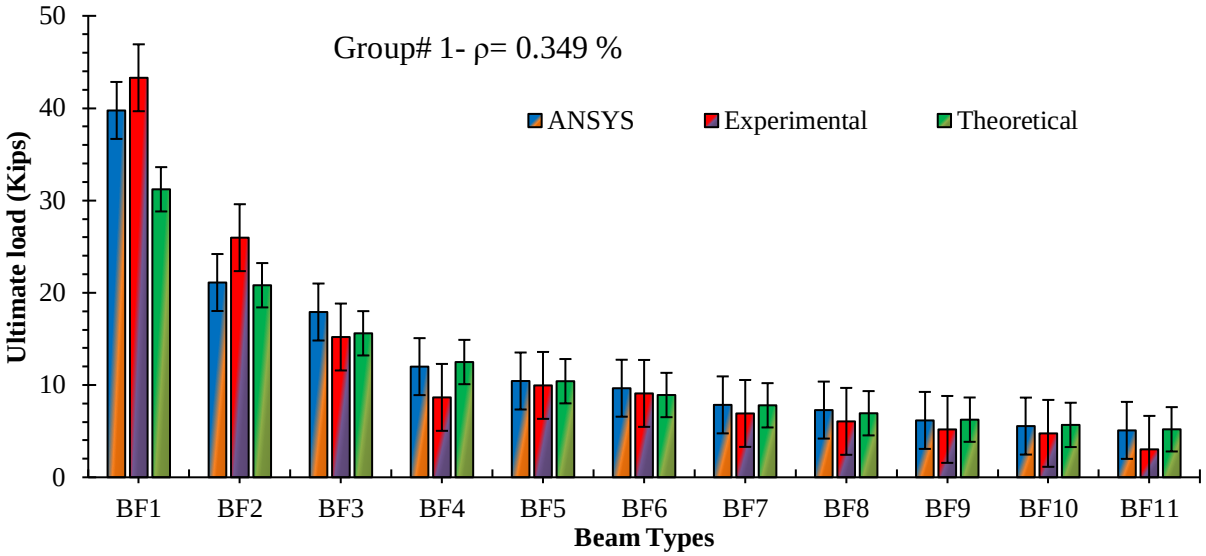

Fig. 16: Comparison of ultimate Load between FEM, experimental and theoretical results for Group No. 01

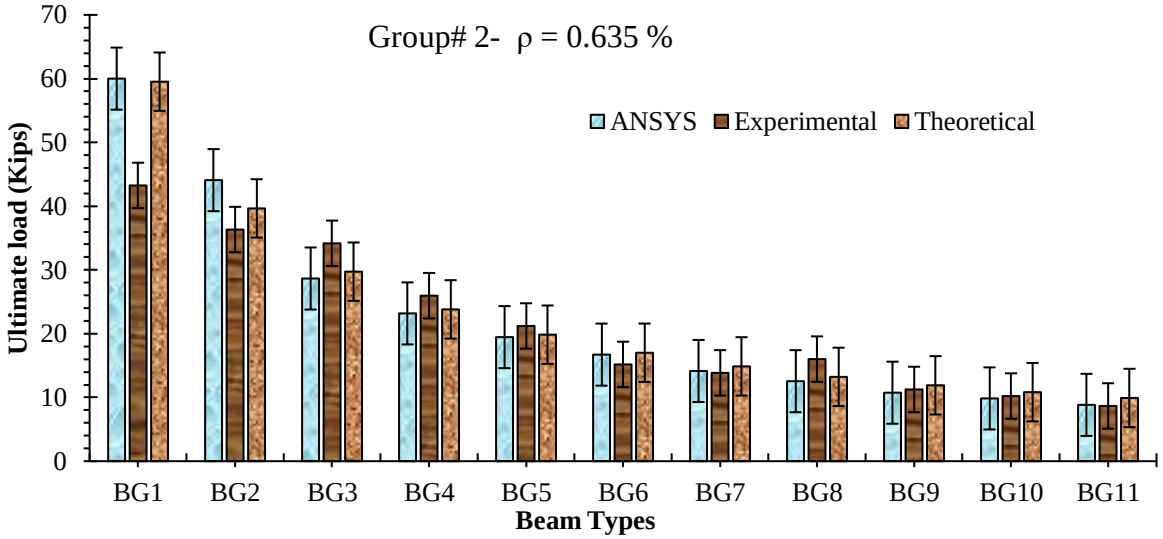

Fig. 17: Comparison of ultimate Load between FEM, experimental and theoretical results for Group No. 02

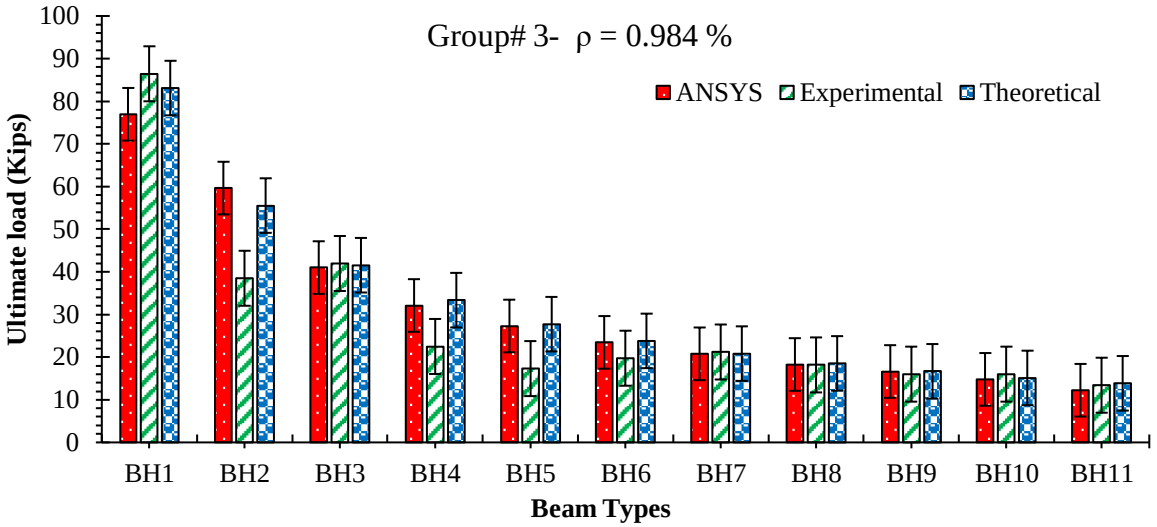

Fig. 18: Comparison of ultimate Load between FEM, experimental and theoretical results for Group No. 03

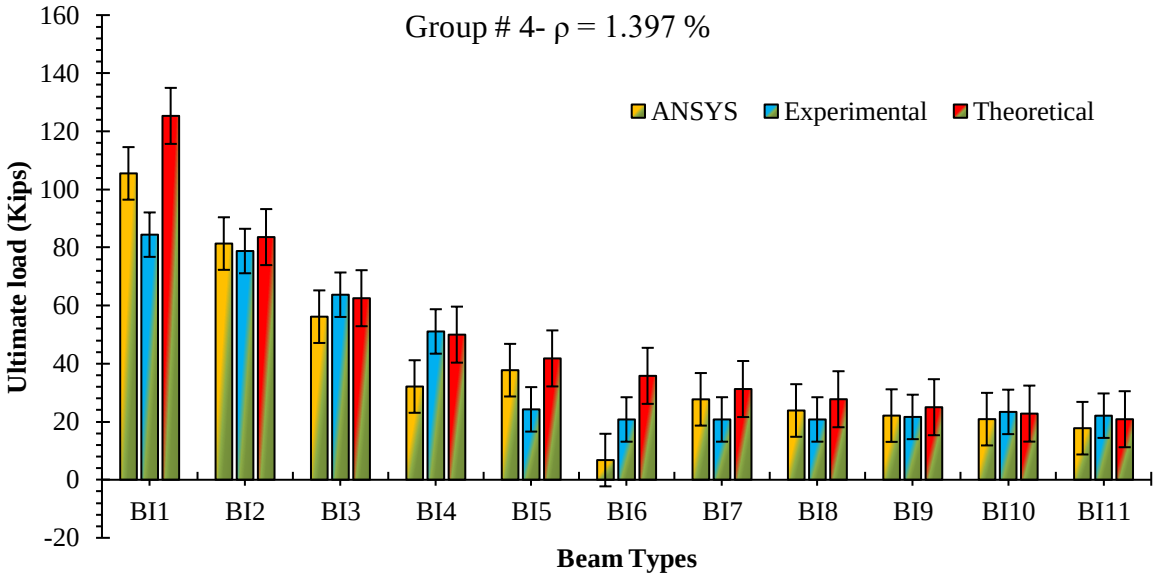

Fig. 19: Comparison of ultimate Load between FEM, experimental and theoretical results for Group No. 04

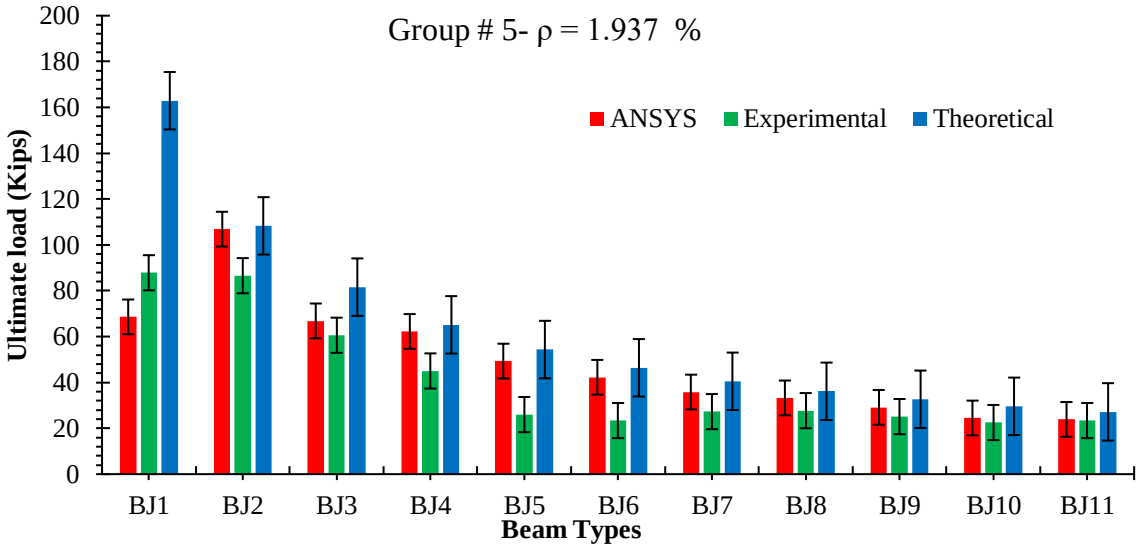

Fig. 20: Comparison of ultimate Load between FEM, experimental and theoretical results for Group No. 05

4.4 Effect of shear span to effective depth ratio (a/d)

4.4.1 Effect of (a/d) ratio on the shear capacity of the beam

Beam specimens with five steel reinforcement ratios have been modeled to examine the shear response of RC beams. It was observed that the FEM results recorded a similar response of the beams tested experimentally; the shear capacity decreased exponentially when the shear span to effective depth (a/d) ratio was increased, as shown in Figure 21.

4.4.2 Effect of (a/d) ratio on relative moment capacity of the beam

For the constant level of steel reinforcement ratio, it was observed that the relative flexural capacity M_{exp}/ M_{theo} or M_{ansys} /M_{theo} normally decreases from a/d =1 to 3, and from 3 to 6, it increases for the constant value of steel ratio, as shown in Figure 22.

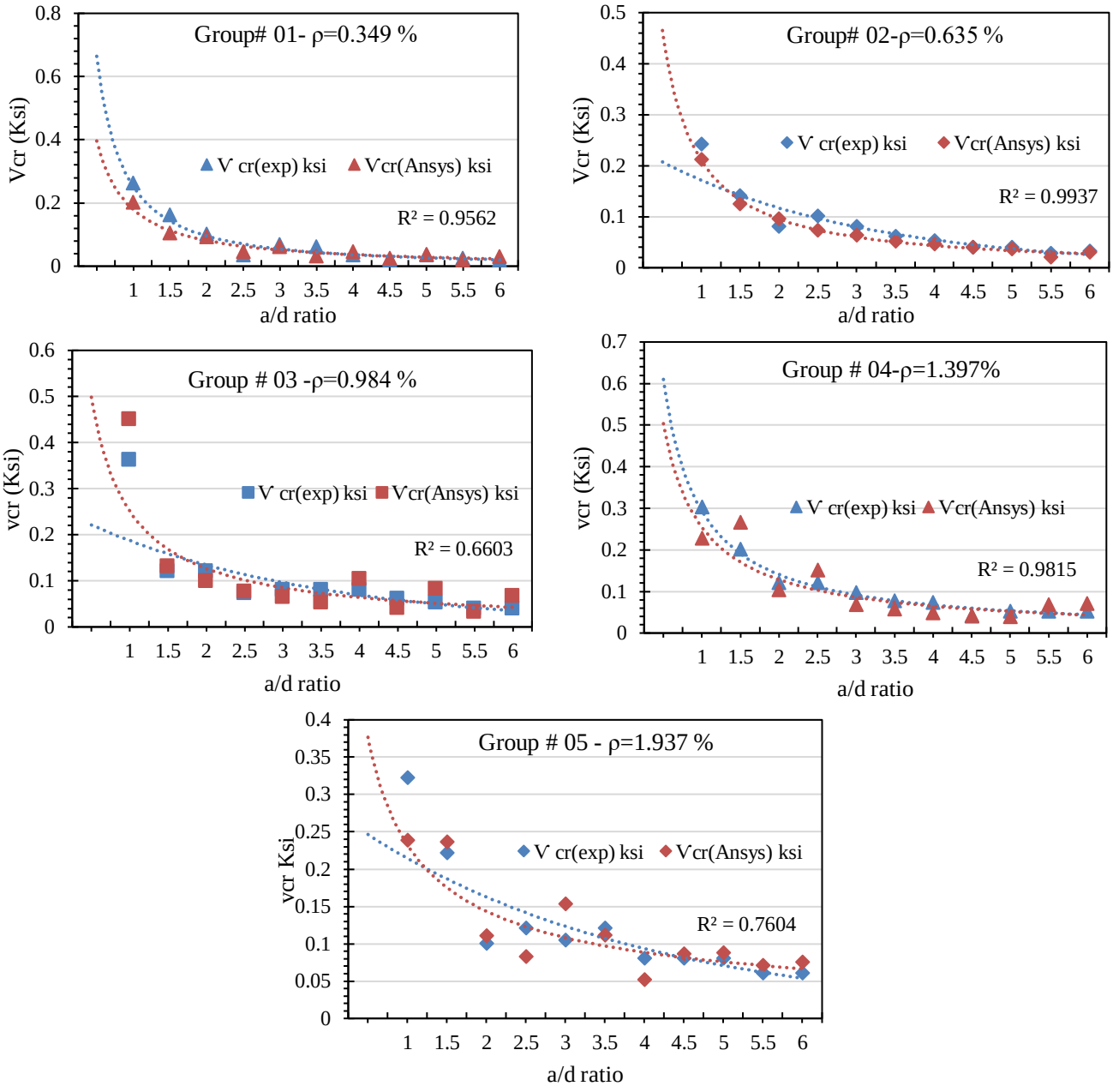

Fig. 21: Comparison of Shear stress at initial cracking between FEM and Experimental results

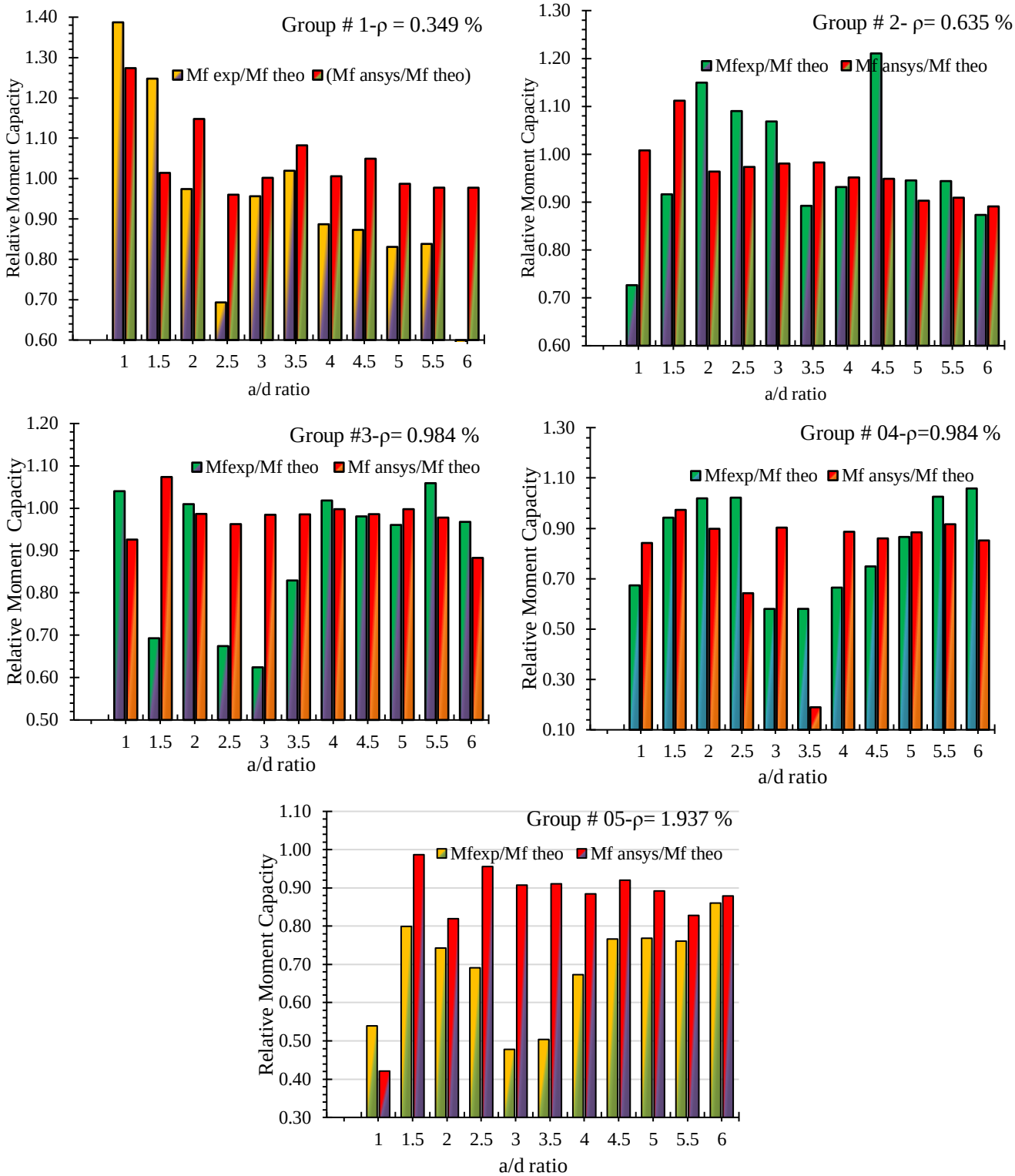

Fig. 22: Comparison of Relative Moment Capacity between FEM and Experimental results

5. Conclusions

Based on the comparative study of FEM and experimental works on RC simply supported beams with different steel reinforcement and shear to depth (a/d) ratios under center-point loading, the following conclusions have been drawn:

1. The FEM results show good agreement with experimental results attained from a reinforced concrete beam with only minor deviations of 5%.
2. At an early stage, the FEM model shows closer results to experimental data than the result obtained at the ultimate loading stage. This may be ascribed to the higher ultimate load of the FEM model, which might be due to the perfect bonding assumption between concrete and reinforcement.
3. By using a constant steel ratio, the parameters P_{cr}, P_u, v_{cr}, *and* v_u are decreased with increasing a/d ratio of the RC beams.
4. Using the constant a/d ratio, the parameters P_{cr}, P_u, v_{cr}, *and* v_u are ameliorated with increasing steel ratio.
5. The relative flexural capacity M_{exp}/ M_{theo} or M_{ansys} /M_{theo} normally decreases from a/d = 1 to 3 and from a/d = 3 to 6, it ameliorates for the constant value of the steel ratio. This may be ascribed to a valley of diagonal shear failure formed in the vicinity of a/d = 3.
6. The proposed FEM model precisely captured the cracking patterns and failure modes of the RC beams. Therefore, this model can be employed for the further parametric study, analysis, and design of RC beams.

References

[1] Demir, A., Ozturk, H., & Dok, G. (2016). 3D numerical modeling of RC deep beam behavior by nonlinear finite element analysis. Disaster Science and Engineering, 2(1), 13-18.

[2] Ahmad, A., & Raza, A. (2020). Reliability analysis of strength models for CFRP-confined concrete cylinders. Composite Structures, 244, Article e112312.

[3] Aslam, H. M. U., Sami, A., & Raza, A. (2021). Axial compressive behavior of damaged steel and GFRP bars reinforced concrete columns retrofitted with CFRP laminates. Composite Structures, 258, Article e113206.

[4] Raza, A., & Ahmad, A. (2021). Investigation of HFRC columns reinforced with GFRP bars and spirals under concentric and eccentric loadings. Engineering Structures, 227, Article e111461.

[5] Raza, A., Nawaz, M. A., & Ahmed, I. (2020). Structural performance of FRP-RC compression members wrapped with FRP composites. Structures, 27, 1693-1709.

[6] Raza, A., & Rafique, U. (2021). Efficiency of GFRP bars and hoops in recycled aggregate concrete columns: Experimental and numerical study. Composite Structures, 255, Article 112986.

[7] Aghabozorgi, P., Khaloo, A., & Hassanpour, S. (2021). Numerical investigation of GFRP bars contribution on performance of concrete structural elements. Numerical Methods in Civil Engineering, 5(4), 1-12.

[8] Danesh, F., & Faridalam, M. (2016), Numerical study on the behavior of link-to-column connections in eccentrically braced frames. Numerical Methods in Civil Engineering, 1(1), 1-6.

[9] Soltani, M., & Sistani, A. (2017). Elastic stability of columns with variable flexural rigidity under arbitrary axial load using the finite difference method. Numerical Methods in Civil Engineering, 1(4), 23-31.

[10] Joshuva, N. R., Saibabu, S., Eapen Sakaria, P., Lakshmikandhan, K. N., & Sivakumar, P. (2014). Finite element analysis of reinforced and pre-tensioned concrete beams. Emerging Technology and Advanced Engineering, 4(10), 449-457.

[11] Uddin, M. A., Alzara, M. A., Mohammad, N., & Yosri, A. (2020). Convergence studies of finite element model for analysis of steel-concrete composite beam using a higher-order beam theory. Structures, 27, 2025-2033.

[12] Kim, S. K., Kim, J. M., & Hong, W. K. (2020). Material nonlinear finite element analysis of hybrid hollow concrete beams encasing steel sections. Structures, 25, 500-519.

[13] Li, C., Li, Q., Li, X., Zhang, X., & Zhao, S. (2020). Elasto-plastic bending behaviors of steel fiber reinforced expanded-shale lightweight concrete beams analyzed by nonlinear finite-element method. Case Studies in Construction Materials, 13, Article e00372.

[14] Dawari, V. B., & Vesmawala, G. R. (2014). Application of nonlinear concrete model for finite element analysis of reinforced concrete beams. Scientific & Engineering Research, 5(9), 776-782.

[15] Srinivasan, R., & Sathiya, K. (2010). Flexural behavior of reinforced concrete Beams using finite element analysis (Elastic Analysis). Buletinul Institutului Politehnic Din Iasi, 56(4), 31.

[16] Raza, A. (2020). Experimental and numerical behavior of hybrid-fiber-reinforced concrete compression members under concentric loading. SN Applied Sciences, 2(4), 1-19.

[17] Elsanadedy, H. M., Al-Salloum, Y. A., Alrubaidi, M. A., Almusallam, T. H., & Abbas, H. (2021). Finite element analysis for progressive collapse potential of precast concrete beam-to-column connections strengthened with steel plates. Building Engineering, 34, Article e101875.

[18] Yu, F., Song, Z., Mansouri, I., Liu, J., & Fang, Y. (2020). Experimental study and finite element analysis of PVC-CFRP confined concrete column–Ring beam joint subjected to eccentric compression. Construction and Building Materials, 254, Article e119081.

[19] Ul Haq, I., Tahir, M. F., Khan, Q. U. Z., Raza, A., & Rizwan, M. (2021). Seismic behaviour of concrete bridge piers with various types of transverse reinforcement. Proceedings of the Institution of Civil Engineers-Structures and Buildings, 1-12.

[20] Wolanski, A. J. (2004). Flexural behavior of reinforced and prestressed concrete beams using finite element analysis. Doctoral dissertation. Marquette University.

[21] Buckhouse, E. R. (1997). External flexural reinforcement of existing reinforced concrete beams using bolted steel channels.

[22] Dahmani, L., Khennane, A., & Kaci, S. (2010). Crack identification in reinforced concrete beams using ANSYS software. Strength of materials, 42(2), 232-240.

[23] Khan, H. U., Rafique, M. N., Karam, S., Ahmad, K., & Bashir, A. (2014). Identification of shear cracks in reinforced beams using finite element method (ANSYS). Pakistan Journal of Science, 66(1), 50.

[24] Tahenni, T., Bouziadi, F., Boulekbache, B., & Amziane, S. (2021). Experimental and nonlinear finite element analysis of shear behaviour of reinforced concrete beams. Structures, 29, 1582-1596.

[25] Carpinteri, A., Carmona, J. R., & Ventura, G. (2011). Failure Mode Transitions in Reinforced Concrete Beams Part 2: Experimental Tests. ACI Structural, 108(3).

[26] Badiger, N. S., & Malipatil, K. M. (2014). Parametric study on reinforced concrete beam using ANSYS. Civil and Environmental Research, 6(8), 88-94.

[27] Patil, S. S., Shaikh, A. N., & Niranjan, B. R. (2013). Experimental and analytical study on reinforced concrete deep beam. Mordern Engineering Research, 3(1), 45-52.

[28] Reddy, G., & Rao, T. M. (2017). Flexural Behaviour of Reinforced Concrete Beams using ANSYS. CVR Journal of Science and Technology, 12, 1-12.

[29] Bahij, S., Adekunle, S. K., Al-Osta, M., Ahmad, S., Al-Dulaijan, S. U., & Rahman, M. K. (2018). Numerical investigation of the shear behavior of reinforced ultra-high-performance concrete beams. Structural Concrete, 19(1), 305-317.

[30] Blomfors, M., Berrocal, C. G., Lundgren, K., & Zandi, K. (2021). Incorporation of pre-existing cracks in finite element analyses of reinforced concrete beams without transverse reinforcement. Engineering Structures, 229, Article e111601.

[31] Alachek, I., Reboul, N., & Jurkiewiez, B. (2019). Experimental and finite element analysis of the long-term behaviour of GFRP-concrete hybrid beams fabricated using adhesive bonding. Composite Structures, 207, 148-165.

[32] Elahi, A. (2003). Effect of reinforcement ratio and shear span on shear strength of high-strength concrete beams. Doctoral dissertation. Taxila University.

[33] William, K. J., & Warnke, E. D. (1975). Constitutive model for the triaxial behaviour of concrete. Association for Bridge and Structural Engineering, 19, 174.

[34] Ibrahim, A. M., & Mahmood, M. S. (2009). Finite element modeling of reinforced concrete beams strengthened with FRP laminates. European Journal of Scientific Research, 30(4), 526-541.

[35] Fanning, P. (2001). Nonlinear models of reinforced and post-tensioned concrete beams. Electronic Journal of Structural Engineering, 1(2), 111-119.

[36] Kachlakev, D. I., Miller, T. H., Potisuk, T., Yim, S. C., & Chansawat, K. (2001). Finite element modeling of reinforced concrete structures strengthened with FRP laminates. Transportation Research Group.

[37] Saifullah, M., Nasir, U., & Udin, S. (2011). Experimental and analytical investigation of flexural behavior of reinforced concrete beam.

[38] Vasudevan, G., & Kothandaraman, S. (2011). Parametric study on nonlinear finite element analysis on flexural behaviour of RC beams using ANSYS. civil & structural engineering, 2(1), 98-111.

Appendix A

A. 1. Theoretical Calculations

Inspection of RC beam for flexural behavior at an applied load of 3,426 lb (see Figure A.1).

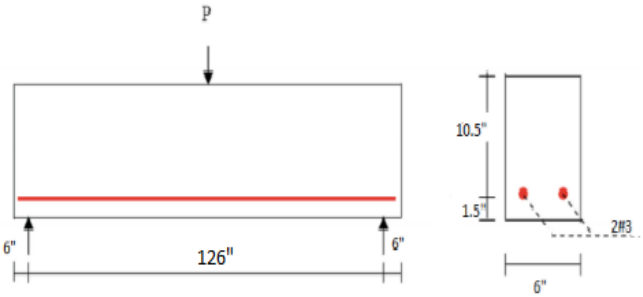

Fig. A.1: RC beam for flexural behavior at an applied load

The moment that develops from the existing forces is the maximum moment.

$$M = \frac{PL}{4} = \frac{3{,}426.126}{4} = 107.919 \text{ lb.in} \quad \text{(A.1)}$$

Properties of Material. The gross moment of inertia (I_G)

$$I_G = \frac{bh^3}{3} = \frac{6.12^3}{3} = 864\ in^4 \quad \text{(A.2)}$$

Stresses in Concrete and Steel.

The transformed moment of inertia of the concrete and steel was used to compute the stresses at the extreme tension fiber (see Figure A.2).

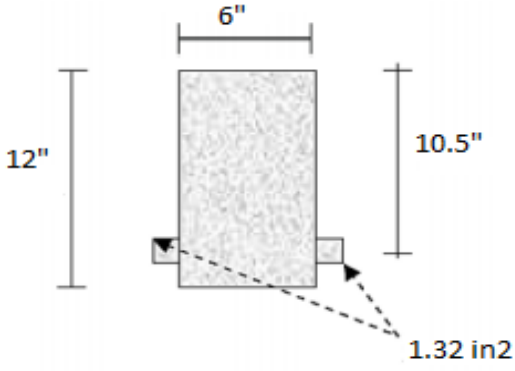

Fig. A.2: Cross-section details of beam

2#3→ ρ = 0.349%, A_s = 0.22 in^2, n = E_s/E_c = 6 (A.3)

Transformed Area of Steel.

$$(A_s)_t = 6.0.22 = 1.32\ in^2 \quad \text{(A.4)}$$

0.66 in^2 distributed at each side of the concrete cross-section.

Distance from the Top Fibre to the Neutral Axis of the Transformed Moment of Inertia:

$$y^- = \frac{A_1 y_1 + A_2 y_2}{A_1 + A_2} = 6.0137\ in \quad \text{(A.5)}$$

Distance between the bottom Fibre to the Elastic Neutral Axis:

$$y_b = 5.986292\ in \quad \text{(A.6)}$$

Transformed Moment of Inertia (I_{tr}):

$$I_{tr} = [I_G + Bd^2]_{conc.} + [Ad^2]_{rebars} = 890.58093\ \text{in}^4 \quad \text{(A.7)}$$

The stress at the extreme tension fiber is:

$$f_{ct} = \frac{M.y_b}{I_{tr}} = \frac{107.919.5.986}{890.58093} = 725.40812\ psi \quad \text{(A.8)}$$

The steel stress at this location is:

$$f_{ct} = \frac{M.y_b}{I_{tr}} n = \frac{107.919.5.986}{890.58093}.6 = 3261.8449\ psi \quad \text{(A.9)}$$

Loads at First Cracking. The load at first cracking:

$$f_{ct} = \frac{M.y_b}{I_{tr}} \quad \text{(A.10)}$$

$$f_{ct} = \frac{PL.y_b}{4I_{tr}} \quad \text{(A.11)}$$

$$725.40812 = P_{cr}\frac{126.5.986}{4.890.58093} \quad \text{(A.12)}$$

$$P_{cr} = 4{,}192\ lbs \quad \text{(A.13)}$$